PCCP

Accepted Manuscript

ROYAL SOCIETY OF CHEMISTRY

www.rsc.org/pccp

Roaming as the Dominant Mechanism for Molecular Products in Photodissociation of Large Aliphatic Aldehydes

Po-Yu Tsai,[1] Hou-Kuan Li,[2] Toshio Kasai,[2,3] and King-Chuen Lin[2,*]

1. **Department of Chemistry, National Chung Hsing University, Taichung 402, Taiwan**
2. **Department of Chemistry, National Taiwan University, Taipei 106, and Institute of Atomic and Molecular Sciences, Academia Sinica, Taipei 106, Taiwan**
3. **Department of Chemistry, Graduate School of Science, Osaka University, Toyonaka, Osaka 560-0043, Japan**

Pages: 34

Figures: 8

Supporting Information

*** To whom correspondence should be addressed.**

Email: kclin@ntu.edu.tw

Fax: 886-2-23621483

Abstract

Photodissociation of isobutyraldehyde (C_3H_7CHO) at 248 nm is investigated using time-resolved Fourier-transform infrared emission spectroscopy to demonstrate the growing importance of roaming pathway with increasing molecular size of aliphatic aldehydes. Each acquired CO rotational distribution from v=1 to 4 is well characterized by a single Boltzmann rotational temperature from 637 to 750 K, corresponding to an average rotational energy of 5.9±0.6 kJ/mol. The roaming signature that shows a small fraction of CO rotational energy disposal accompanied by a vibrationally hot C_3H_8 co-fragment is supported by the theoretical prediction. The energy difference between tight transition state (TS) and roaming saddle point (SP) is obtained to be -27, 4, 15, 22, and 30 kJ/mol for formaldehyde, acetaldehyde, propionaldehyde, isobutyraldehyde, and 2,2-dimethyl propanal, respectively. The roaming SP is stabilized by a larger alkyl moiety. It is suggested that the roaming photodissociation rate of aldehydes increasingly exceeds those via tight TS, resulting in dominance of the CO + alkane products, as the size of aldehydes becomes larger. Along with formaldehyde, acetaldehyde, and propionaldehyde, isobutyraldehyde is further demonstrated that this aldehyde family is the first case for organic compound with special functional group to follow predominantly a roaming dissociation pathway, as the molecular size becomes larger.

1. Introduction

Aldehydes are organic compounds that are widespread in nature. The photolysis of aliphatic aldehydes is an important source of free-radical production in polluted urban atmospheres. When these molecules are irradiated with UV light, the S_1 (n, $\pi^*)_{CO}$ state is promoted, then followed by dissociation into (1) radical fragments (HCO + alkyl) from triplet state T_1 via intersystem crossing (ISC), and (2) molecular products (CO + alkane) from ground state S_o via internal conversion (IC). However, for the molecular channel, the conventional transition state (TS) mechanism, on which chemical reaction and photodissociation have long relied as the foundation, is insufficient to account for the energy flow and branching fraction of the fragments. Recent studies on aliphatic aldehydes have found that reactants are likely to bypass conventional TS forming the same products. Formaldehyde (H_2CO) and acetaldehyde (CH_3CHO) were well characterized to proceed via roaming route as an alternative mechanism in the photodissociation.[1-7] The CO product following the tight TS pathway gains relatively large translational and rotational energy, but the alkane co-product carries small vibrational energy. In contrast, CO via the roaming process is characterized with a slow speed, small rotational energy disposal, whereas alkane is highly vibrationally excited.

Like the tight TS mechanism, a roaming saddle point (SP) has been found individually for a series of aldehydes,[8,9] each showing a very small imaginary (harmonic) frequency along with some small frequency modes. For instance, for CH_3CHO, two weakly bound radical moieties of CH_3 and CHO in the roaming SP are likely to meander around varied configurations along a plateau region of intrinsic reaction coordinate (IRC), prior to abstraction reaction.[9,10] In the roaming SP of propionaldehyde, the H atom of CHO oscillates slowly between two far-separated CHO and CH_3CH_2 moieties.[10] The H abstraction by CH_3CH_2 thus results in weak restoring force that is exerted to CO causing a small torque and subsequently a small rotational energy deposition. The H_2CO configuration evolving along a plateau-like IRC shows a significant increase for transition-mode frequencies towards the product and thus the corresponding dividing surface becomes increasingly narrower and

deeper.[11] The roaming branching fraction varies with excitation energy. When the excitation energy further increases, a triple fragmentation (alkyl+CO+H) might open to hinder roaming identification.[6,12,13]

The branching fractions of roaming/TS pathway to molecular channel in formaldehyde and acetaldehyde at 308 nm were determined to be 10/90% and 84/16%, respectively,[1,2] while the roaming branching in propionaldehyde was reported to be even larger.[10] This work further demonstrates the roaming mechanism as the predominant route for photodissociation of larger size of aliphatic aldehydes. Time-resolved Fourier-transform infrared (FTIR) emission spectroscopy was employed to probe the CO fragment in 248 nm photolysis of isobutyraldehyde (CH_3CH_3CHCHO),[6,14,15] in conjunction with theoretical calculations to identify the roaming signature and to clarify dynamical complexity.

2. Experimental

The experimental process with time-resolved Fourier-transform infrared (FTIR) emission spectroscopy has been described in detail elsewhere.[6,10,14,15] In brief, we mixed 0.5 Torr CH_3CH_3CHCHO in the presence of Ar at 3 Torr in the reaction chamber that was then irradiated at 248 nm. The fragment emission signals were guided to the entrance of the FTIR spectrometer which was operated in a step-scan mode; the movable mirror of interferometer was controlled to move step-by-step. The digitized signals which were repeatedly collected for 30 laser shots were monitored with an InSb detector cooled at 77 K. The output was then fed into a 200 kHz 16-bit transient digitizer for signal processing, which restricted the temporal resolution of IR signal at 5 μs. The obtained interferograms were finally Fourier transformed to yield time-resolved spectra. The spectral responses of beamsplitter, optical filters, and detection system were all calibrated using an IR emitter serving as a blackbody-like radiation.

3. Computational Method

With the aid of electronic structure computation, the kinetic and dynamic features of isobutyraldehyde (CH_3CHCH_3CHO) on the S_0 surface are investigated. GAMESS electronic structure package was utilized to perform all the single/multi-reference electronic structure calculations and *ab initio* classical trajectory simulation.[16,17]

(A) Determination of stationary points

The tight saddle points (SPs) of double and triple fragmentation pathways were evaluated by single-reference *ab initio*/DFT methods. The minima and tight SPs related to these pathways are determined utilizing B3LYP hybrid functional with 6-311++G(d,p) basis set, and the energy is further refined by CR-CC(2,3) /6-311++G(d,p)[18,19] with B3LYP/6-311++G(d,p) zero-point energy (ZPE) correction.

The roaming SPs and related dissociation paths were calculated by utilizing multi-configurational SCF methods. The geometries of roaming SPs were optimized at CASSCF(12e,11o)/6-311++G(d,p) level and the energies were refined by Nakano's second order multi-reference perturbation theory[20] ((12e,11o)-MRMP2/6-311++G(d,p)) with ZPE from CASSCF calculation. Active space are chosen by selecting three C-C σ/σ* orbitals, a pair of OC—H σ/σ* orbitals, a pair of C=O π/π*(C=O) orbitals and a nonbonding orbital on oxygen.

The energy difference between roaming SPs and radical asymptotic limit was evaluated similarly by performing the (12e,11o)-MRMP2/6-311++G(d,p) calculations at a HCO----C_3H_7 distance of 100 Bohr with both fragments in their equilibrium geometries, due to the lack of size consistency in MRMP2 method.[21] Then, the energy information of roaming SPs was combined together with the results of other stationary points from CR-CC(2,3) calculations. The nature of stationary points is examined by the number of imaginary mode (0 for minima and 1 for first-order SPs) from vibrational analysis and also by IRC calculation. For non-stationary geometries along the IRC path, the 3N-7 normal modes and projected vibrational frequencies

which are orthogonal to gradients were computed.[22] All the required nuclear gradients and CASSCF state-specific Hessians were calculated in analytical manner, while the DFT Hessians were all computed numerically via central difference of gradients with a displacement size of 0.01 Bohr.

(B)Reaction rate calculations

We utilize statistical reaction rate theory to evaluate the unimolecular dissociation rate constants for various routes. The dissociation rate constants via tight SPs and roaming SPs are computed by using Rice–Ramsperger–Kassel–Marcus (RRKM) and variational RRKM treatment, respectively.[23] For a complicated molecule like isobutyraldehyde, it is quite difficult to define a global dividing surface incorporating all the saddle points in the same product; thus, the rate constant for each SP is calculated independently. Despite lack of the detailed sketches of transition state, the present results obtained independently for each route may provide qualitative information on the relative rates of various pathways. For eliminating difference of electronic structure calculations by various methods, the required harmonic vibrational frequencies of both reactant and SPs are all computed at CASSCF/6-31++G(d,p) level, while the energy information of each pathway is still adopted from the results of CR-CC(2,3) and MRMP2.

The selection of active spaces in stationary points is described as follows. Minima of parent molecule and SPs along the CO + C_3H_8 channel: π/π* C-O, σ / σ* C-C, σ /σ* C-H and n(O) in CO (CASSCF(8e,7o)); SP of three-body break-up channel: π/π* C-C, σ/σ* C-C, σ/σ* H-H, π/π*CO and n(C) in CO (CASSCF(10e,9o)). For applying variational RRKM treatment to roaming SPs, the harmonic frequencies of the projected 3N-7 vibrational modes at various configurations along the IRC path are also computed. The vibrational state-counting are approximated in terms of free-rotor energy levels for those low-frequency normal modes (below 100 cm^{-1}) in either SPs or minima. Among the five transitional modes of each roaming SP, however, few of them are larger than 100 cm^{-1} in most IRC grids. In order to avoid discontinuity in state-counting results along IRC by the switch between vibration and free-rotor

treatments, free-rotor approximation is applied only to the three lowest transitional modes of a roaming SP in the variational RRKM calculations.

(C)Dynamical simulation

ab initio "on the fly" direct dynamical calculation is performed for all the CO-forming molecular channels by utilizing the DRC (dynamic reaction coordinate) code[24] of GAMESS. All the classical trajectories initiated from SPs toward molecular products are evaluated at CASSCF(10e,9o)/6-31+G(d) level, with the active space being chosen in the following manner. SP of three-body break-up: π /π* C-C, σ/σ* C-C, σ/σ* H-H, π/π*CO and n(C) in CO; tight SP of CO + propane (C_3H_8) channel: three pairs of σ/σ* C-C bonds, two π of CO and another π* (C=O); roaming SP: similar to CASSCF(12e,11o) calculation but without n(O) orbital. To save the computational time, both the active space and the basis functions are reduced but without scarifying the reliability of results. In the roaming pathways, for example, we remain two C-C bonding/antibonding pairs on propane in active space, in order to appropriately describe the influence of the propane backbone on the large stretching motion of C-H bond to which >80% impulsive energy is released. To understand how the excess energy of 45.4 kcal/mol above the SPs ZPE, equivalent to one-photon energy of 248 nm, is partitioned into the CO vibrational states, trajectories calculations for various dissociation routes are performed under two initial conditions as follows. (1) Starting from minimum energy path (MEP) without excess energy included. But an initial kinetic energy of 0.1 kcal/mol is given at each SP geometry to run the trajectory. (2) Starting from roaming SP with excess energy. Both stationary points have the same active space. The energy difference (including ZPE from CASSCF(10e,9o)/6-31+G(d) calculation) is evaluated by the (10e,9o)-MRMP2/6-31+G(d) calculation level.

Because the computational efficiency of *ab initio* direct dynamic calculation is much less than QCT calculation on analytic PES function, we adopted a simple treatment with highly-contracted phase space to obtain initial condition for proceeding trajectories. The number of trajectories is largely reduced, but computational

reliability is still remained. All the trajectories start at the configuration of roaming SP, while the excess energy is randomly distributed to each vibrational normal mode according to their harmonic vibrational frequencies. For an N-atomic molecule with 3N-7 real modes, the average quanta $<n_i>$ in the normal mode i is evaluated from a probability distribution, $P(n_i)$. Such a probability distribution for each normal mode can be obtained by calculating the number of states, while assuming the residual energy is randomly distributed to other 3N-8 modes after the n_i-quanta excitation in mode i. Once the $<n_i>$ of 3N-7 real modes are calculated by direct-counting algorithm, the residual kinetic energy along the reaction coordinate (E_{rc}) is expressed by

$$E_{rc} = E_{excess} - \sum_{i=1}^{3N-7} E_i \qquad (1)$$
$$E_i = \langle n_i \rangle v_i$$

Though the initial conditions of all trajectories remain at the same E_{rc} and {Ei} values, the relative phases between normal modes are different in each trajectory. For a polyatomic molecule such as isobutyraldehyde with totally 32 real modes, there are 2^{32} different combinations to be chosen. Further simplification is made by dividing normal modes into several groups according to their vibrating characters. The real normal modes of isobutyraldehyde is divided into seven groups: (a) five transitional modes with relative motion of HCO and C_3H_7 fragments; (b) nine C-C vibrational modes; (c) eight C-H bending modes; (d) seven C-H stretching modes; (e) bending mode in HCO; (f) CH mode in HCO, and (g) CO mode in HCO. The initial relative phases between vibrational modes within the same group are chosen to possess most probable combination. The number of positive phases in a group of n vibrational modes is either n/2±1/2 for odd n or n/2 for even n. Therefore, it further reduces the possible numbers of combination.

4. Results and Discussion

(A) Internal energy disposal in CO and C_3H_8

Upon irradiation at 248 nm, the CO fragment dissociated from CH_3CH_3CHCHO in the presence of Ar was acquired with time-resolved FTIR emission spectroscopy. An example is given in Fig.1, showing the observed CO (v=1-4) spectrum, in the range of 1900-2200 cm^{-1} with a 0.25 cm^{-1} resolution, in 0 μs delay with respect to the laser firing; a spectral simulation is accompanied for comparison. As restricted to the instrument response time of 5 μs, the spectrum obtained at 0 μs delay is actually an average over the 0-5 μs duration. The population for each rotational line in the time-resolved spectra is determined with given Einstein spontaneous emission coefficients. In the experiment, 3 Torr of Ar gas corresponds to a number density of 1.1×10^{17} molecules/cm^3. The relative speed between C_3H_7CHO and Ar at 300 K is estimated to be ~$5x10^4$ cm/s. Given the collision cross section of 35 $Å^2$, the fragments as detected within 1 μs have been exposed to ~18 collisions with Ar. The CO fragment is apparently rotationally relaxed. The rotational population for each vibrational state from v=1 to 4 can be fitted satisfactorily with a single Boltzmann distribution. Then, a semi-logarithmic plot of $\ln[N_{v,J}/(2J+1)]$ versus $E_{v,J}$ yields the corresponding rotational temperature. The rotational population in each v may be well characterized with a single Boltzmann rotational temperature. Here, $N_{v,J}$ is the relative population of CO in the (v, J) level and $E_{v,J}$ is the rotational energy. The nascent rotational temperature of CO (v=1-4) is determined to be in the range of 637-750 K by extrapolating the time-dependent rotational temperatures to the real zero time based on the method of curve fitting.[6,10] As listed in Table 1, the rotational energy $E_{rot}(v)$ may be evaluated to be 6.2, 5.5, 5.6, and 5.3 kJ/mol for v=1, 2, 3, and 4, respectively, by

$$E_{\mathrm{rot}}(v) = \sum_{J=1}^{J=\max} P_{v,J} E_{v,J} , \qquad (2)$$

where $P_{v,J}$ is the fraction of molecules populated in the J level. By summing up each rotational line at a given v, time-dependent vibrational population is obtained and the vibrational population ratio at different time delay may then be estimated. While taking into account $E_{rot}(v)$ with the vibrational population ratio at 2.5 μs delay (the

average of 0 to 5 μs) and assuming vibrational relaxation is negligible within 2.5 μs, the CO rotational energy is averaged to be 5.9±0.6 kJ/mol.

Note that the rotational populations are very efficiently thermalized. Leone group reported that the CO rotational distribution from photolysis of acetone at 193 nm was measured with a similar technique and the ir vibration-rotation spectrum of CO acquired in the 6-30 μs delay time was observed to change significantly within a single gas kinetic collision.[25] Thus, it is crucial to avoid CO collisions with the partners. By extrapolating to the real zero delay time free from the Ar collisions, the CO rotational population is likely to be in a nascent state, and thereby the nascent rotational temperature can be obtained. For instance, the CO rotational distribution obtained in the 248 nm photolysis of CH_3COCl (ref.26) and $CH_2BrCOCl$ (ref.27) following similar processes as this work gave rise to rotational temperature of about 300 K and 1200-1470 K, respectively, corresponding to the rotational energy of 2.4 and 9.2 kJ/mol. Despite acquisition of the same CO fragment in the photolysis, the resulting CO rotational temperature depends significantly on the type of molecules. Thus, the rotational temperature of 637-750 K determined in this work may well be considered to be (almost) nascent.

In addition, the time-resolved FTIR method is sensitive enough to distinguish different rotational population components, if any, with the aid of spectral simulation in which the rotational population is characterized by Boltzmann law due to a μs instrument response time. For instance, with the same method, a bimodal rotational distribution of CO (v=1) dissociated from acetaldehyde at 308 nm was obtained.[28] The time-dependent ratio of low-/high-J component is then extrapolated to a real zero time at which the collision effect by Ar is removed. The obtained ratio of (10±2)/(90±5)% at v=1 is consistent with the value of 13/87% for CO at v=1 by Houston and Kable with laser-induced fluorescence method.[2] The bimodal feature also shows a reasonable trend as compared to the values of 20/80%(ref.5) and (15±3)/(85±12)%(ref.7) for CO (v=0) at 308 nm reported previously using resonance-enhanced multiphoton ionization spectroscopy (REMPI) coupled with ion-imaging. Such consistency is indicative of reliability of the branching evaluation

without suffering from the collision interference.

As shown in Fig.2, a Boltzmann plot of $\ln(P_{vib})$ versus $(-E_{vib}/k_B)$ at 2.5 μs delay yields a straight line with the slope corresponding to $1/T_{vib}$, and thus the vibrational temperature is obtained to be 6100±300 K. Here, P_{vib} denotes the fraction of vibrational population (v=1-4) and E_{vib} is the vibrational energy. At this temperature, the fraction of vibrational population at each v (from 0 to 4) may be evaluated and the CO vibrational energy was then evaluated to be 41±3 kJ/mol with zero-point energy included. The results are summarized in Table 2. The CO fragment is obtained vibrationally hot and rotationally cold.[10]

As shown in Fig.3a, the rotation-vibration spectrum of C_3H_8 is acquired in the spectral range from 2500 to 3050 cm^{-1}. Following the same procedure reported previously,[6,28] the portion of rotational energy, assumed to have equal contribution for the parallel- and perpendicular-type rovibrational transitions of symmetric top at 500 K, is removed from the spectrum yielding a pure vibrational spectrum (Fig.3b). It is found that the pure vibrational spectrum is very similar to the raw data, and is much less influenced by variation of rotational temperature, because C_3H_8 owns small rotational constants (0.97, 0.28 and 0.25 cm^{-1}). As reported, C_3H_8 contains 27 modes. Among them, 6 CH_3-stretch modes and 2 CH_2-stretch modes have the fundamental vibrational frequencies from 2887 to 2977 cm^{-1},[29] that appear in the vibrational spectrum acquired. A high-resolution FTIR spectrum of C_3H_8 was recently obtained at 215 K showing the above fundamental stretching modes from 2850 to 3025 cm^{-1}.[30] As compared to the results by Harrison and Bernath,[30] the obtained pure vibrational spectrum is greatly red shifted from 2850 to 2500 cm^{-1}, apart from the fundamental emission from v=1 to 0 (Fig.3b). The large red-shifted region is indicative of the ir emission transitions from higher vibrational states (v≥2), in which anharmonic character is inherent. The complicated spectrum of C_3H_8 hinders the possibility of quantitative estimate of the vibrational energy disposal. However, the large red shift of the emission transition suggests that the C_3H_8 co-product must be highly vibrationally excited in the photolysis of isobutyraldehyde.

(B) Isomerization and photodissociation pathways

The minima of isobutyraldehyde on the S_0 surface are optimized comprising gauche- and trans-isomers. Fig.4 shows the pathways connecting these conformers. The global minimum is at the gauche-form configuration which consists of a pair of enantiomers (MIN1 and MIN1', 0 kJ/mol). These two enantiomers can either isomerize to each other via a route with barrier height of 5.73 kJ/mol, or evolve to the trans-form at the local minimum (MIN2, 1.27 kJ/mol) by surpassing the related SPs (ISO-TS 1 and ISO-TS 1', 3.65 kJ/mol), respectively.

Fig.5a shows the photodissociation pathways of isobutyraldehyde to the related radical and molecular channels on the S_0 surface. The CO fragments are evaluated to result from the following routes: (1) CH_3CH_3CHCHO in gauche-form (or (2) in trans-form) is dissociated directly to CO + C_3H_8 via a tight TS at 344.2 (or 351.6) kJ/mol, and (3) the same precursor undergoes three-body dissociation to C_3H_6 + H_2 + CO via a TS at 300.3 kJ/mol or (4) to C_3H_7 + H + CO. The propylene (C_3H_6) fragment owns a CH_3 asymmetric (ν_{15}) and CH_2 asymmetric stretch mode (ν_1) at 2950 and 3090 cm^{-1} with a large Einstein spontaneous emission coefficient of 5.6 and 3.9 s^{-1}, respectively.[31] As shown in Fig.3, the ν_{15} mode at 2950 cm^{-1} overlaps with the Q branch of C_3H_8, but the ν_1 mode appears at 3090 cm^{-1} with a weak intensity. Thus, we cannot exclude the CO contribution from the three-body dissociation channel (C_3H_6 + H_2 + CO). Despite appearance of triple fragmentation (H + CO + CH_3) in CH_3CHO at 248 nm,[6] this channel was evidenced experimentally to be negligible in propionaldehyde.[10] The distinction can be rationalized. The available energy in photodissociation tends to distribute statistically to each radical fragment (HCO + alkyl) which is generated from the energized S_0 state. The alkyl moiety with larger vibrational degrees of freedom is allowed to gain larger internal energy. Thus, there is not enough internal energy left in HCO to undergo decomposition. Photodissociation of isobutyraldehyde at 248 nm is likewise free from interference of triple fragmentation (H+CO+C_3H_7). Even for smaller aldehyde like CH_3CHO dissociated at 248 nm, the vibrational population distribution of CO via triple fragmentation, H +

$CO + CH_3$, was evaluated by a prior model,[6,32,33] yielding a population ratio of 0.942 : 0.057 : 0.00079 : 0 for v=0, 1, 2, and 3. The CO population at v≥1 dissociated from this channel may well be neglected as compared to that at v=0.

As with smaller aliphatic aldehydes,[9,10] two roaming SPs, CH_3CHCH_3…CHO, for the pair of enantiomers were found in isobutyraldehyde (Fig.5b), showing a common feature to have five low-frequency transitional modes closely associated with the relative motion between radical moieties. The H atom of HCO abstracted by CH_3CHCH_3 at a long distance excites the newly-formed C-H bond exclusively, thus resulting in large vibrational energy deposited in C_3H_8 and small rotational energy in CO due to a weak torque generated by the departing H. In contrast, for the tight TS structure, simultaneous fission/formation of C-H bonds is likely to generate large translational and rotational energies partitioning to C_3H_8 + CO (Fig.5a). Note that we did not succeed in finding the H-roaming SP around CH_3CHCH_3CO core.[7]

To characterize the energy flow for roaming and tight TS pathways, QCT calculations were performed on the individual SP configurations (tight1, triple, and RM2 (gauche form)) with zero excess energy. The energy disposals for each fragment calculated are shown in Fig.6 and Table.3. The roaming CO product carries small translational and rotational energy fractions (4.1% and 6.0%), whereas C_3H_8 gains large vibrational energy fraction (80.6%). In contrast, CO following the tight TS gains relatively large translational and rotational energy fractions (40.7% and 16.9%), but C_3H_8 obtains small vibrational energy fraction (37.5%). The fragments via three-body dissociation (H_2+CO+C_3H_6) gain large translational energy fraction (75.4%), small CO rotational energy fraction (9.19%), and extremely small CO vibrational energy fraction (0.09%). The trend of energy distribution (Fig.6) for roaming and tight TS mechanisms is essentially consistent with those reported previously.[1-7,10-12] Further, the predicted trend of a small fraction of CO rotational energy disposal accompanied by highly vibrationally excited C_3H_8 co-product is consistent with the observation, thus confirming the dominance of roaming mechanism leading to the products, CO + C_3H_8, in photodissociation of isobutyraldehyde at 248 nm. The feature of a single rotational component with small rotational energy deposited is similar to that found in

the case of propionaldehyde,[10] but differs from a bimodality observed in acetaladehyde. We also observe existence of three-body dissociation channel (C_3H_6 + H_2 + CO), but the CO contribution cannot be differentiated from the roaming pathway. The aspects might be speculated. First, the CO contribution from three-body dissociation is small and thus hard to be discerned in the rotational energy distribution. Second, the rotational energy fraction is similar between these two sources and their rotational distributions overlap to a large extent such that they are hard to be clearly separated.

The molecular photodissociation lifetime of CH_3CHO was reported to be < 5 ns at 312 nm under jet-cooled temperature ~1 K.[34] However, in our work with an effusive beam at ~300 K, the molecules may have chance to populate in different vibrational modes and levels of the excited state upon the laser irradiation. Different vibrational modes and levels result in different molecular symmetric properties which can dramatically change the dissociation efficiency. When the precursor is populated in some vibrational modes with slowed predissociation processes, the collision-induced IC has chance to give rise to new dissociation fragments. For instance, in the 248 nm photodissociation of the C_2H_5COCl molecular beam heated to 153 ^oC, the major fast dissociation channel of C–Cl bond fission was accompanied by a minor channel of HCl elimination which proceeded on the ground state.[35] In contrast, the HCl elimination was not observed in a supersonic molecular beam at cold temperature.[36]

While inspecting the case of CH_3CHO reported previously,[37-40] the fragments produced via the S_0 pathway are expected to follow a sequential ISC path: $S_1 \rightarrow S_1/T_1$ ISC$\rightarrow$ $T_1 \rightarrow$ T_1/S_0 ISC$\rightarrow S_0$. The S_1/S_0 IC process seems to play a minor role. The molecular channel CO + CH_4, if generated along these ISC-based routes, retains a small available energy partitioning in the fragments such that the CO population may lie in low vibrational states. In contrast, this work was conducted under the condition of higher Ar pressure. The CO product in C_3H_7CHO is obtained vibrationally hot, different from that in CH_3CHO.[37-40] In addition to the ISC-based process, the Ar collision-induced level-to-level coupling rate between S_1 and the dramatically

increased density of states in S_0 at higher excitation energy like 248 nm may be enhanced more rapidly than S_1-T_1 coupling. Thus, a large available energy is likely remained for the molecular channel and CO may gain larger vibrational excitation energy.

To understand the discrepancy between experimental and calculated results, we perform direct dynamical calculations with the excess energy above the ZPE of roaming SP equivalent to the excitation energy at 248 nm, while the CO fragment remains initially at either state of v=0, 1, and 2. Because of time-consuming, a total of 18 trajectories were computed, comprising 10, 6, and 2 trajectories for the initial C=O mode set at v=0, 1, and 2, respectively. The obtained fractions of product energy disposal for CO(v=0-2)+C_3H_8 are given in Fig.7, similarly showing the trend consistent with roaming dynamical signature; CO has a very low rotational energy fraction along with a small center-of-mass translational energy fraction, while C_3H_8 is highly vibrationally excited. The CO vibrational excitation remains surprisingly the same as the initial CO mode prepared, indicating that no impulse is exerted on CO vibration. If the excess energy is assumed to be statistically partitioned into initial CO vibrational degree of freedom, the CO vibrational temperature is estimated to be 1175±52 K, still much less than the observation. The discrepancy might be associated with the fact that the minimum energy path could be curved.[41,42] The curvature along the reaction path is likely to cause the coupling between the reaction coordinate and the transverse modes.[41,42] Such a coupling effect is neglected in the direct dynamical calculations herein. Another possibility is that the effect of collision-induced IC is not taken into account in the simulation. Therefore, performing QCT calculations on constructed ground-state or multi-state PESs should be required, for incorporating possibly the non-statistical effect in the CO mode during the roaming motion.

Apart from the QCT calculations, the rate constants for each reaction channel are further estimated. The roaming SP is lower by 29.7 (36.2) kJ/mol than the tight TS associated with the trans-form (gauche-form). According to variational RRKM method,[23] Fig.8 shows the excitation-energy dependence of the dissociation rate constants in which the roaming rate constant gains an order of 10^9 cm^3/molecule/s at

482 kJ/mol (or 248 nm), much larger than 10^6 and 10^7 cm^3/molecule/s for the tight TS pathways of two-body and three-body dissociation, respectively.

Note that the rate constant calculations regarding the tight TS, roaming SP, and free radical pathways were treated dynamically independent. In fact, the roaming pathway stems from the radical channel on the ground state surface and thus dynamically competes with each other. Hindrance effect is one of the effective factors to change their rates. For instance, between the cases of CH_3CHO and H_2CO, a steric effect induced by the CH_3 group in CH_3CHO may hinder H abstraction from HCO, thereby slowing down the roaming reaction rate. To inspect the hindrance influence, Kable and coworkers thus defined a parameter P as a ratio of the sum of roaming SP states to the sum of radical product states. It was determined to be 1 in H_2CO and 0.21 in CH_3CHO.[43] The roaming rate constant in CH_3CHO is thus reduced by a smaller P in order to fit the observed branching ratio of roaming/radical pathway. Despite the fact that a larger aldehyde may suffer from larger hindrance along the roaming pathway, it is found that lowering the energy state of the roaming SP, with respect to the tight TS, increases significantly the contribution of roaming mechanism. The roaming SP in C_3H_7CHO, which is stabilized by a larger C_3H_7 moiety, appears much lower in energy than the tight TS, thereby resulting in dominance of the $CO+C_3H_8$ products.

In order to systematically compare the energy difference between tight TS and roaming SP for various aldehydes, we include a larger size of aldehyde, 2,2-dimethyl propanal ($CH_3C(CH_3)_2CHO$). Its structures of tight TS and roaming SP are depicted in Fig.1S in Supporting Information with detailed description of the calculation procedure. We perform single point energy calculations from formaldehyde to 2,2-dimethyl propanal to remain a consistent trend of energy difference between tight and roaming SPs. The B3LYP/6-311++G(3df,3dp) energies are calculated for molecular structures which are optimized at B3LYP/6-311++G(d,p) level with the zero-point energies computed via 6-311++G(d,p) basis set. The roaming SPs of aldehydes are found to be slightly below the related asymptotic radical; thus, we simply consider the energy gap between tight SP and radical limit, but neglect the tiny

energy difference. In this manner, the energy difference is obtained to be -27, 4, 15, 22, and 30 kJ/mol for formaldehyde, acetaldehyde, propionaldehyde, isobutyraldehyde, and 2,2-dimethyl propanal, respectively. The tight TS of formaldehyde is stabilized by a deep attractive potential well of H-H diabatic curve, whereas the roaming SP is stabilized by a larger alkyl moiety. The results show a trend that the energy difference between tight SP and radical limit increases with the molecular size. It is suggested that the roaming photodissociation rate of aldehydes increasingly exceeds those via tight TS, resulting in dominance of the CO+alkane products, as the size of aldehyde becomes larger.

5. Conclusion

Photodissociation of isobutyraldehyde (C_3H_7CHO) at 248 nm is investigated to demonstrate the growing importance of non-transition state (TS) dynamics with increasing molecular size of aliphatic aldehydes. Time-resolved Fourier-transform infrared (FTIR) emission spectroscopy was employed to probe the resulting CO and C_3H_8 fragments in conjunction with theoretical calculations to clarify dynamical complexity. From experimental and theoretical evidences, the roaming mechanism in isobutyraldehyde has been characterized to be the dominating route to the molecular channel of CO + alkane. The tight TS mechanism is negligible as the aliphatic aldehyde becomes larger.

Acknowledgement

This work is supported by Ministry of Science and Technology, Taiwan, Republic of China under contract no. NSC 102-2113-M-002-009-MY3.

References

1. D. Townsend, S. A. Lahankar, S. K. Lee, S. D. Chambreau, A. G. Suits, X. Zhang, J. Rheinecker, L. B. Harding, and J. M. Bowman, *Science*, 2004, **306**, 1158.
2. P. L. Houston and S. H. Kable, *Proc. Nat. Acad. Sci. USA*, 2006, **103**, 16079.
3. L. Rubio-Lago, G. A. Amaral, A. Arregui, J. G. Izquierdo, F. Wang, D. Zaouris, T. N. Kitsopoulos, and L. Banares, *Phys. Chem. Chem. Phys*., 2007, **9**, 6123.
4. B. R. Heazlewood, M. J. T. Jordan, S. H. Kable, T. M. Selby, D. L. Osborn, B. C. Shepler, B. J. Braams, and J. M. Bowman, *Proc. Nat. Acad. Sci. USA*, 2008, **105**, 12719.
5. L. Rubio-Lago, G. A. Amaral, A. Arregui, J. Gonzalez-Vazquez, and L. Banares, *Phys. Chem. Chem. Phys.* 2012, **14**, 6067.
6. K.-C. Hung, P.-Y. Tsai, H.-K. Lee, and K.-C. Lin, *J. Chem. Phys.* 2014, **140**, 064313.
7. K. L. K. Lee, M. S. Quinn, A. T . Maccarone, K. Nauta, P. L. Houston, S. A. Reid, M. J. T. Jordan, and S. H Kable, *Chem. Sci.* 2014, **5**, 4633.
8. L. B. Harding, S. J. Klippenstein, and A. W. Jasper, *Phys. Chem. Chem. Phys.* 2007, **9**, 4055.
9. B. C. Shepler, Y. Han, and J. M. Bowman, *J. Phys. Chem. Lett.* 2012, **2**, 834.
10. P.-Y. Tsai, K.-C. Hung, H.-K. Li, and K.-C. Lin, *J. Phys. Chem. Lett.* 2014, **5**, 190.
11. P.-Y. Tsai and K.-C. Lin, *J. Phys. Chem. A*, 2015, **119**, 29.
12. P. -Y. Tsai, M.-H. Chao,T. Kasai, K.-C. Lin, A. Lombardi, F. Palazzetti, and V. Aquilanti, *Phys. Chem. Chem. Phys.*, 2014, **16**, 2854.
13. P. Morajkar, A. Bossolasco, C. Schoemaecker, and C. Fittschen, *J. Chem. Phys.* 2014, **140**, 214308.
14. Y.-Y. Yeh, M.-H. Chao, P.-Y. Tsai, Y.-B. Chang, M.-T. Tsai, and K.-C. Lin, *J. Chem. Phys.* 2012, **136**, 044302.
15. E.-L. Hu, P.-Y. Tsai, H. Fan, and K.-C. Lin, *J. Chem. Phys.* 2013, **138**, 014302.
16. M. W. Schmidt, K. K. Baldridge, J. A. Boatz, S. T. Elbert, M. S. Gordon, J. H.

Jensen, S. Koseki, N. Matsunaga, K. A. Nguyen, S. J. Su, T. L. Windus, M. Dupuis, and J. A. Montgomery, *J. Comput. Chem.* 1993, **14**, 1347.

17. M. S. Gordon and M. W. Schmidt, In "Theory and Applications of Computational Chemistry: The First Forty Years", C. E. G. Frenking, K. S. Kim, G. E. Scuseria, Eds.; Elsevier: Amsterdam, 2005, pp 1167– 1190.
18. P. Piecuch, S. A. Kucharski, K. Kowalski, and M. Musial, *Comput. Phys. Commun.* 2002, **149**, 71.
19. P. Piecuch and M. Wloch, *J. Chem. Phys.* 2005, **123**, 224105.
20. H. Nakano, *J. Chem. Phys.* 1993, **99**, 7983.
21. J. M. Rintelman, I. Adamovic, S. Varganov, and M. S. Gordon, *J. Chem. Phys.* 2005, **122**, 044105.
22. W. H. Miller, N. C. Handy, and J. E. Adams, *J. Chem. Phys.* 1980, **72**, 99.
23. L. Zhu and W. L. Hase, RRKM, a General RRKM program, 1993.
24. M. S. Gordon, G. Chaban, and T. Taketsugu, *J. Phys. Chem.* 1996, **100**, 11512.
25. E. L. Woodbridge, T. R. Fletcher, and S. R. Leone, *J. Phys. Chem.* 1988, **92**, 5387.
26. Y-T. Liu, M-T. Tsai, C-Y. Liu, P.-Y. Tsai, K. C. Lin, Y. H. Shih, and A. H. H. Chang, *J. Phys. Chem. A* 2010, **114**, 7275.
27. C.-Y. Liu, M.-T. Tsai, P.-Y. Tsai, Y.-T. Liu, K. C. Lin, S. Y. Chen, and A. H. H. Chan, *ChemPhysChem.* 2011, **12**, 206.
28. H-K. Li, P-Y. Tsai, K.-C. Hung, T. Kasai, and K. C. Lin, *J. Chem. Phys.*, 2015, **142**, 041101.
29. NIST/TRC Web Thermo Tables, professional edition (thermophysical and thermochemical data).
30. J. J. Harrison and P. F. Bernath, *J. Quant. Spec. Rad. Trans.* 2010, **111**,1282.
31. E. Es-sebbar, M. Alrefae, and A. Farooq, *J. Quant. Spec. Rad. Trans.* 2014, **133**, 559.
32. M. Hunter, S. A. Reid, D. C. Robie, and H. Reisler *J. Chem. Phys.* 1993, **99**, 1093.
33. J. T. Muckerman, *J. Phys. Chem.* 1989, **93**,179.
34. S. H. Lee and I. C. Chen, *Chem. Phys.* 1997, **220**, 175.

35. L. R. McCunn, M. J. Krisch, K. Takematsu, L. J. Butler, and J. N. Shu, *J. Phys. Chem. A* 2004, **108**, 7889.

36. Z. R. Wei, X. P. Zhang, W. B. Lee, B. Zhang, and K. C. Lin, *J. Chem. Phys.* 2009, **130**, 014307.

37. G. A. Amaral, A. Arregui, L. Rubio-Lago, J. D. Rodriguez, and L. Banares, *J. Chem. Phys.*, 2010, **133**, 064303.

38. B. R. Heazlewood, S. J. Rowling, A. T. Maccarone, M. J. T. Jordan, and S. H. Kable *J. Chem. Phys.* 2009, **130**, 054310.

39. R. Heazlewood, A. T. Maccarone, D. U. Andrews, D. L. Osborn, L. B. Harding, S. J. Klippenstein, M. J. T. Jordan, and S. H. Kable, *Nature Chemistry* 2011, **3**, 443.

40. F. Gherman, R. A. Friesner, T.-H. Wong, Z. Min, and R. Bersohn *J. Chem. Phys*. 2001, **114**, 6128.

41. W. H. Miller, N. C. Handy, and J. E. Adams, *J. Chem. Phys.*1980, **72**, 99.

42. Page and J. W. McIver, *J. Chem. Phys.,* 1988, **88**, 922.

43. U. Andrews, S. H. Kable, and M. J. T. Jordan, *J. Phys. Chem. A*, 2013, **117**, 7631.

Table.1 Rotational temperature (K) and rotational energy disposal of CO (v=1-4)

t(μs)	v=1	v=2	v=3	v=4	$\langle E_{rot} \rangle$[3]
2.5	720	650	600	600	
7.5	650	600	550	600	
12.5	600	550	500	470	**5.9 kJ/mol**
17.5	500	450	500	450	
nascent T_{rot}[1]	**750**	**662**	**670**	**637**	
E_{rot} (kJ/mol)[2]	**6.2**	**5.5**	**5.6**	**5.3**	

[1.] Nascent rotational temperatures T_{rot} are determined by extrapolating the time-dependent rotational temperautre to t=0.

[2.] Rotational energy of each CO(v) state is calculated by assuming Boltzmann rotational population at given rotational temperature.

[3.] Vibrationally-averaged rotational energy is calculated by using nascent Erot and vibrational population at t=2.5 μs (assuming vibrational relaxation is negligible within 2.5 μs) for CO v=1~v=4.

Table.2 Vibrational population, temperature and energy of CO (v=1-4)

t(μs)	v=1	v=2	v=3	v=4	$<E_v>$[1]
2.5	0.477	0.239	0.115	0.081	**41±3 kJ/mol**
7.5	0.498	0.224	0.124	0.070	T_{vib}
12.5	0.510	0.219	0.112	0.071	**6100±300 K**
17.5	0.501	0.216	0.125	0.070	

1. Vibrational energy is calculated by using T_{vib}=6100 K Boltzmann distribution of v=0 to v=4 (normalized up to v=4) and vibrational eigenvalues (including ZPE) of v=0 to 4 calculated via the same set of molecular constants in spectral simulation. $<E_v>$ is reported in kJ/mol

Table.3 Product energy distribution (PED) of three minimum energy path (MEP) trajectories in percentage (%) (see Fig.6). Et, Ev, and Er represent translational, vibrational, and rotational energy, respectively. C_3H_x denotes the corresponding hydrocarbon product from each pathway.(x=8 for Tight TS and Roam SP, x=6 for Triple-body fragmentation)

	Et	Ev(CO)	Er (CO)	Ev(HH)	Er (HH)	Ev(C_3H_x)	Er(C_3H_x)
Tight	**40.73**	**2.50**	**16.92**	**0**	**0**	**37.47**	**2.37**
Triple	**75.35**	**0.09**	**9.19**	**0.41**	**0.07**	**8.42**	**6.47**
Roam	**4.09**	**0.24**	**5.99**	**0**	**0**	**80.58**	**9.10**

Figure Captions

Fig.1 Comparison between simulation and observed spectrum acquired in 0 μs delay with respect to the laser firing. As restricted to the instrument response time, the spectrum obtained at 0 μs delay is actually an average over the 0-5 μs duration.

Fig.2 A Boltzmann plot of $\ln(P_{vib})$ against $(-E_{vib}/k_B)$ yields the CO vibrational temperature. P_{vib} and E_{vib} denote the CO vibrational population (v=1-4) and the corresponding vibrational energy, respectively. The reciprocal of the slope from least-squares-fit is the vibrational temperature.

Fig.3 (a) Ir rotation-vibration spectrum of C_3H_8. (b) pure vibration spectrum of C_3H_8 in comparison with the absorption spectrum obtained by Harrison and Bernath under a condition of 215 K and 52.01 Torr (ref.30). A large red shift of the emission transition indicates that the molecule is highly vibrationally excited.

Fig.4 Interconversion between two gauche forms through a trans-form with related barrier energies.

Fig.5 (a) Threshold energies (kJ/mol) and reaction pathways of radical and molecular channels on C_3H_7CHO S_0 surface. (b) Structures of roaming SPs and intrinsic reaction coordinate of trans-form roaming path. The formyl group proceeds flipping motion along the reaction path. Geometry optimization were performed via CASSCF(12e,11o)/6-311++G(d,p). Energies were calculated by (12e,11o)MRMP2/6-311++G(d,p).

Fig.6 Bar plot of relative energy disposals of isobutyraldehyde dissociation along different pathways. The CO product via the roaming SP (tight TS) gains 6.2% (19.4%) available energy that is partitioned to the vibrational and

rotational fractions of 0.24% (2.5%) and 6.0% (16.9%), respectively. Meanwhile, C_3H_8 obtains 89.7% (39.8%) available energy that is distributed to vibration (80.6%(37.5%)) and rotation (9.1%(2.4%)). The roaming products gain a translational energy fraction of 4.1%, whereas the tight TS products obtain 40.7%. The C_3H_6 + H_2 + CO channel gains a fast speed (75.4% translational energy fraction) with a small fraction (9.19%) of CO rotational energy and a very small fraction (0.09%) of CO vibrational energy.

Fig.7 Fraction of product energy distribution (PED%) as a function of different types of energy disposal. Direct dynamical calculations of roaming pathway with the excess energy equivalent to the photolysis energy at 248 nm. The trajectories are initiated from the roaming SP with CO mode prepared initially at either state of v=0, 1, and 2. The C_3H_8 co-product is highly vibrationally excited, gaining a fraction up to 90%. In contrast, CO gains a vibrational energy fraction of 12% for the initial state prepared at v=2, remaining almost the same energy disposal as the initial state. CO has a very small rotational energy fraction <4%. The other 2-4% available energy is released to translational degree of freedom. In the figure, E_t, E_v, and E_r denote translational, vibrational, and rotational energy partition, respectively.

Fig.8 Energy dependence of RRKM and variational RRKM rate constants associated with five pathways: tight CO (gauche- and trans-form), H_2 + CO + C_3H_6 (gauche-form), and roaming pathways (gauche- and trans-form).

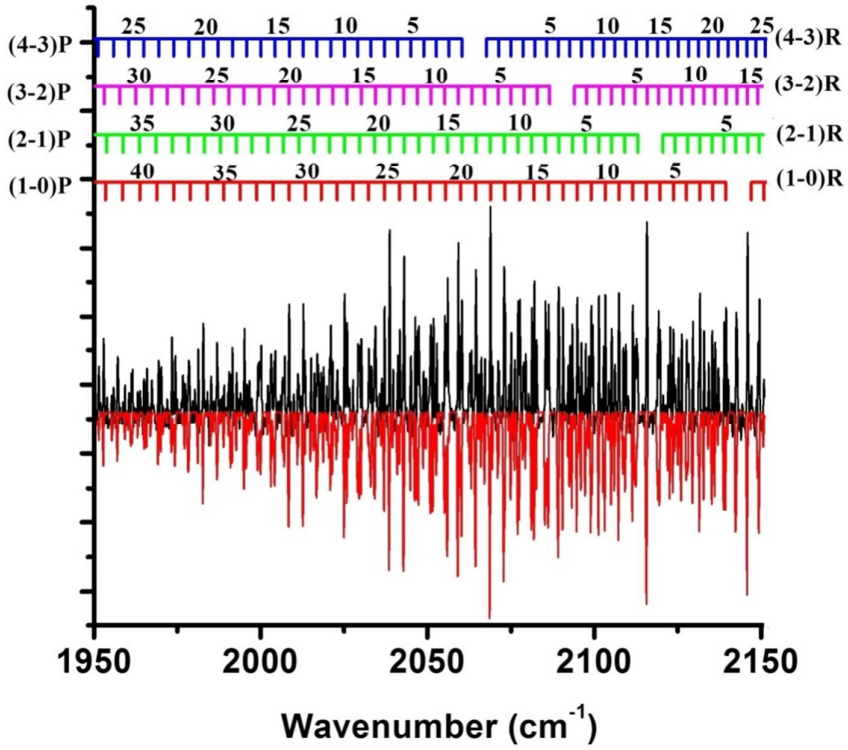

Fig.1

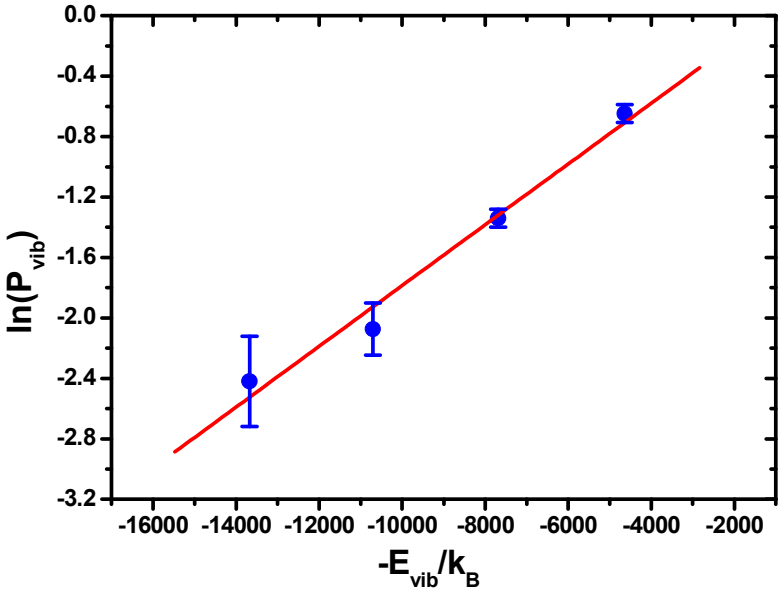

Fig.2

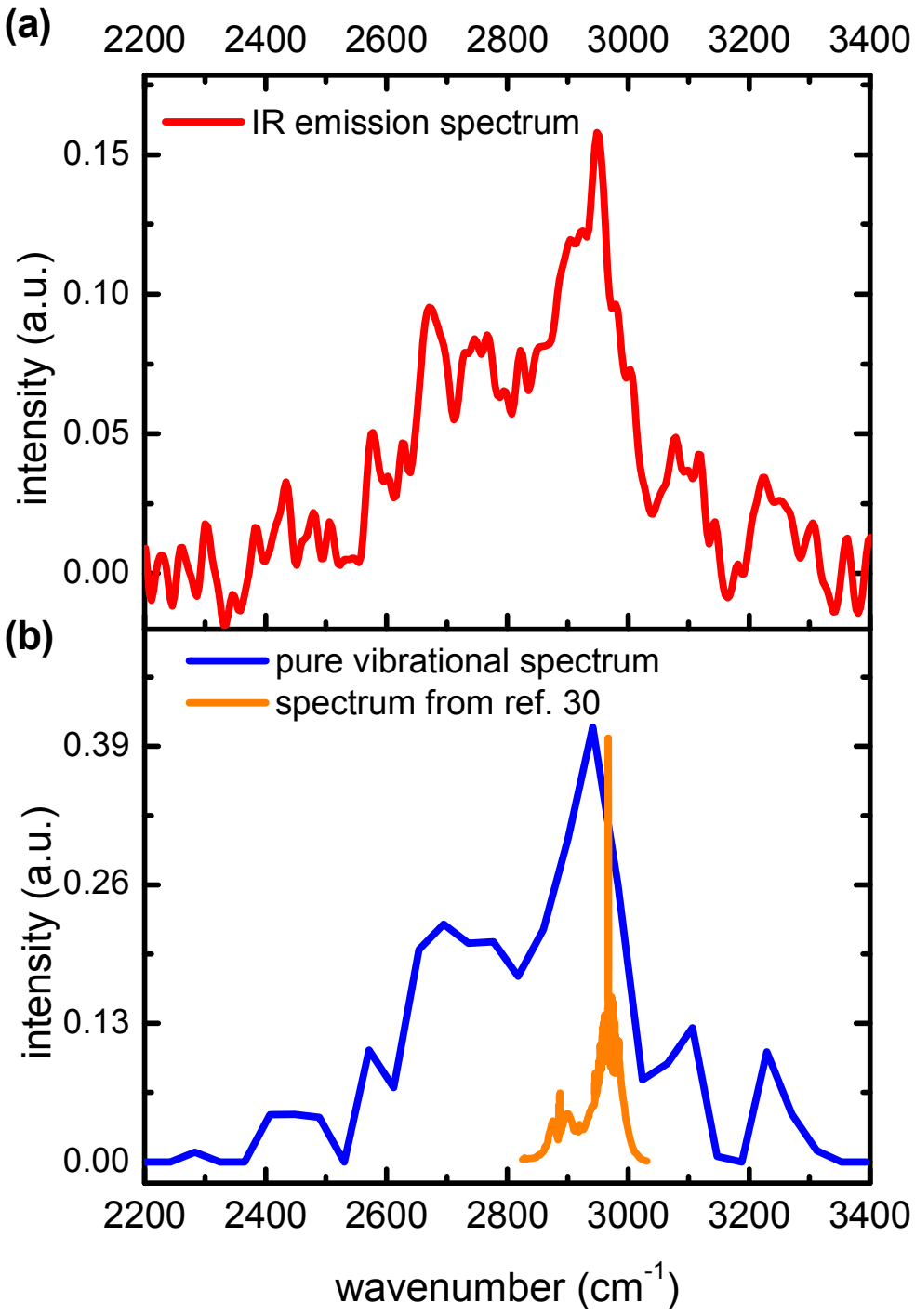

Fig.3

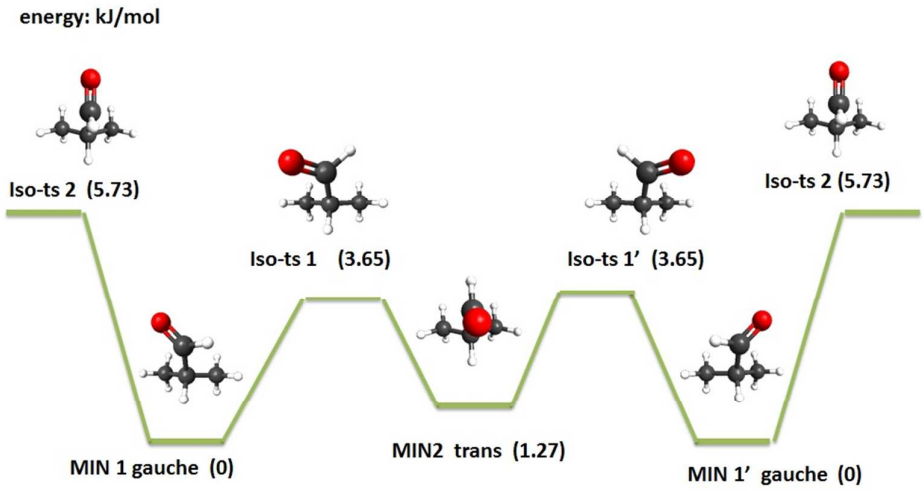

Fig.4

(a)

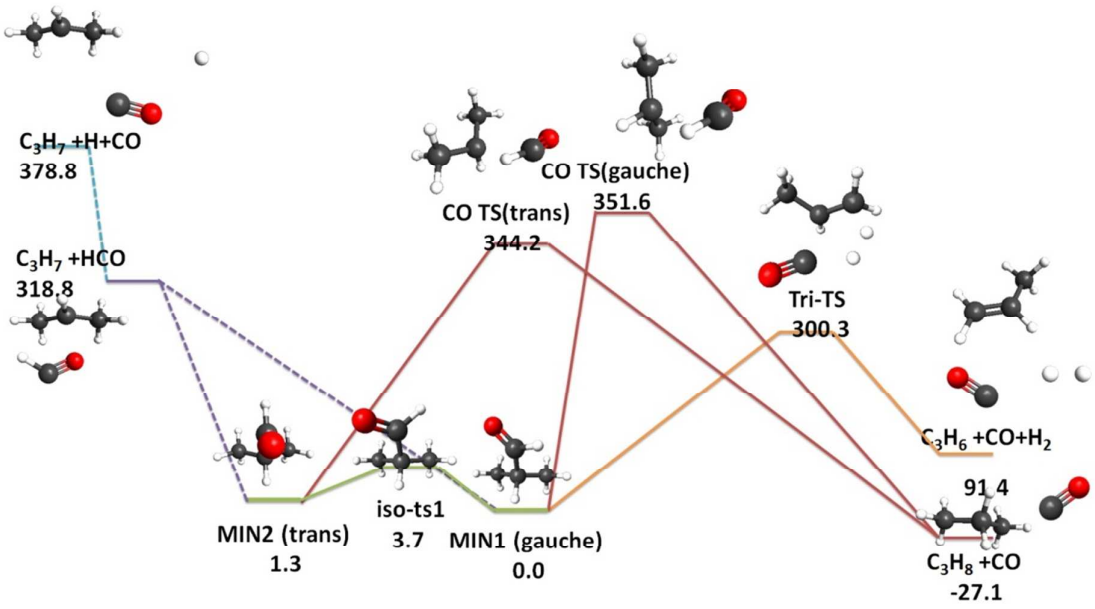

(b)

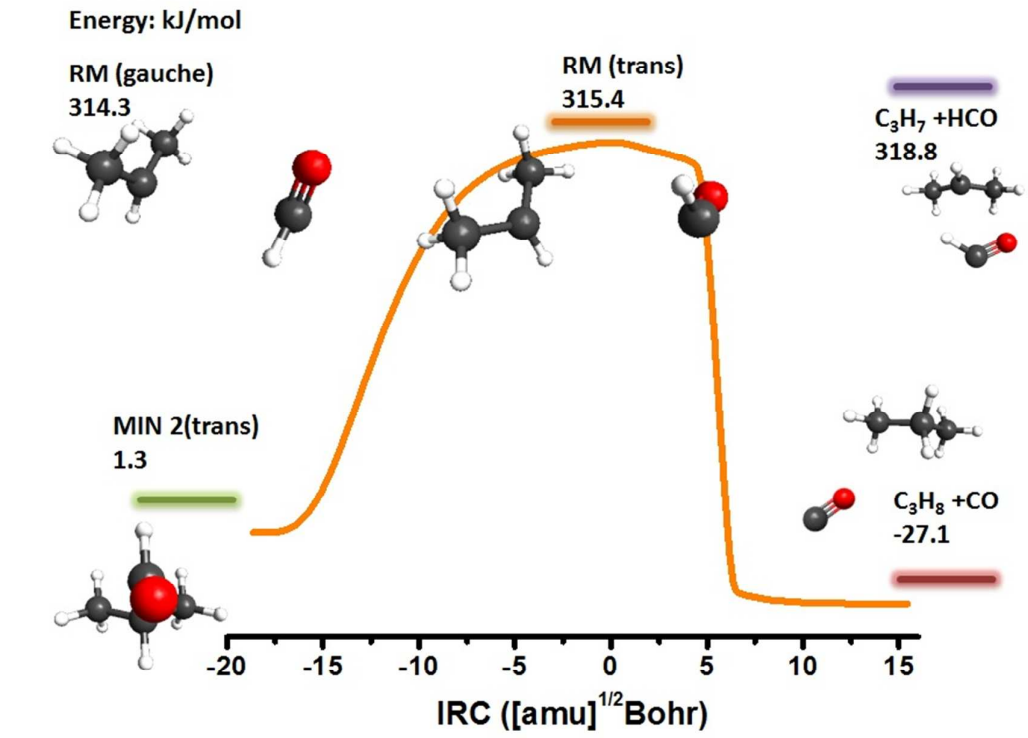

Fig.5

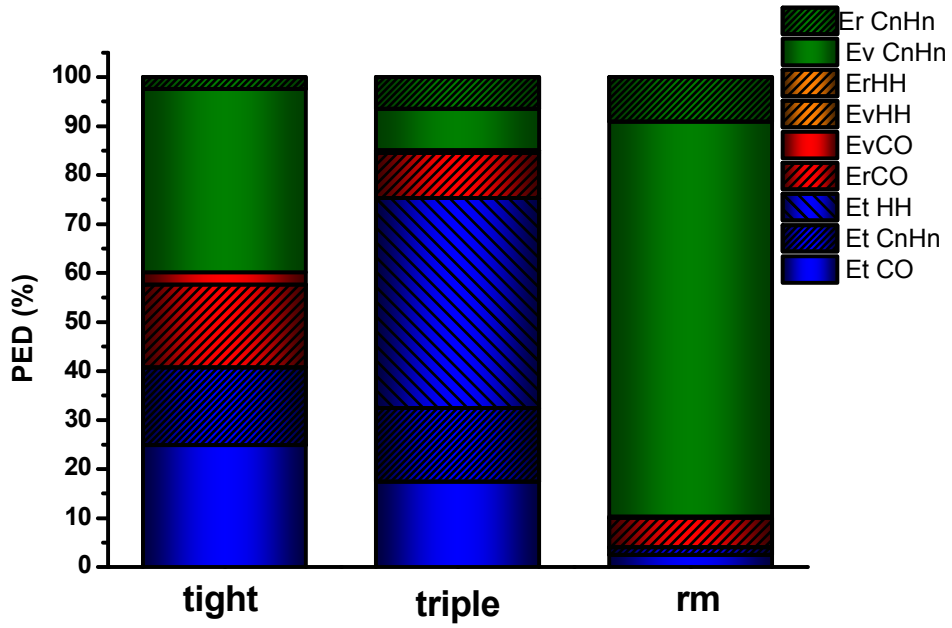

Fig.6

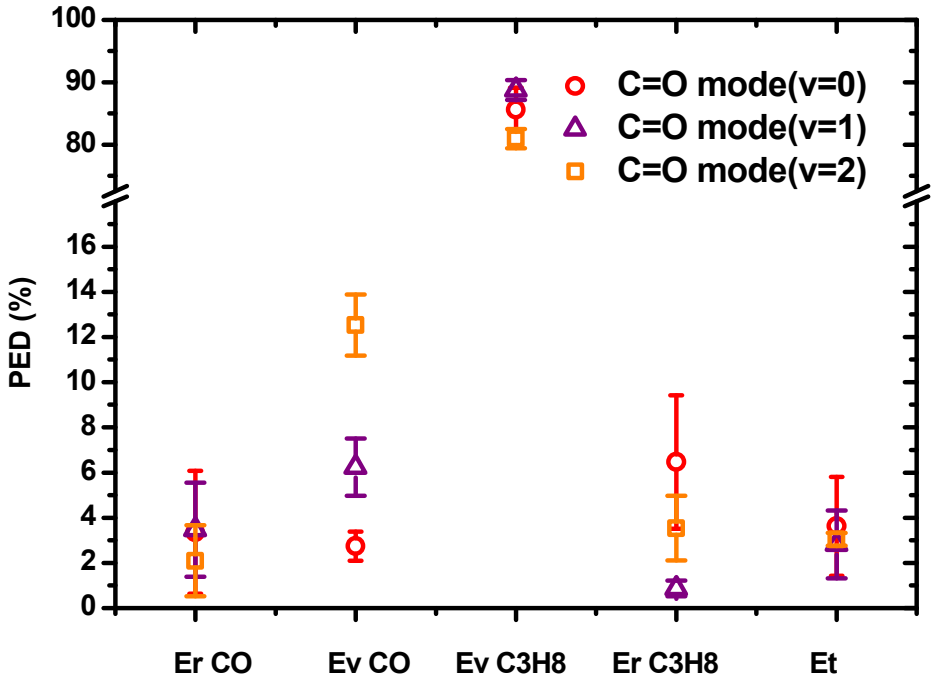

Fig.7

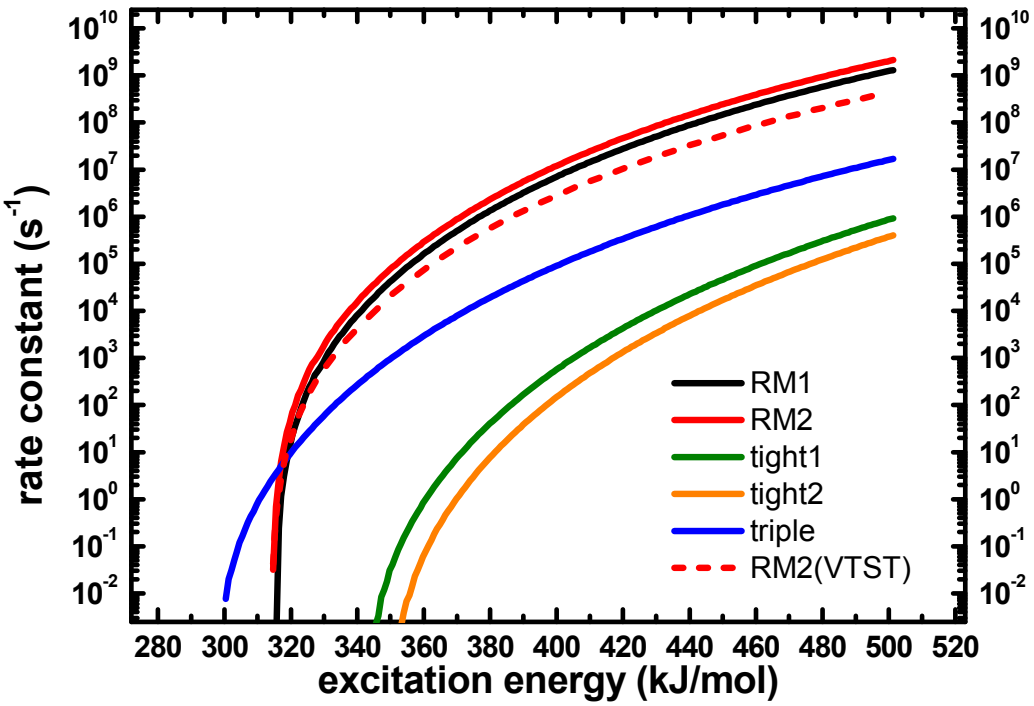

Fig.8